Applications in Engineering Science 1 (2020) 100002

Contents lists available at ScienceDirect

Applications in Engineering Science

journal homepage: www.elsevier.com/locate/apples

Linear stability analysis of blood flow in small vessels

L. Fusi, A. Farina*

Universitá degli Sudi di Firenze Dipartimento di Matematica e Informatica "U.Dini", Viale Morgagni 67/A, Firenze 50134, Italy

ARTICLE INFO

Keywords:
Linear stability
Blood flow
Microvessels

ABSTRACT

We investigate the linear stability of unidirectional Poiseuille flow of blood modeling the fluid as a spatially inhomogeneous fluid in which viscosity depends on the red blood cell concentration (RBCs). We consider small vessels like arteries terminal branches, arterioles or venules, where the inhomo-geneity is due to the non uniform distribution of RBCs on the vessel cross section. The stability analysis is performed applying the classical normal-mode linear analysis which results in a fourth-order eigenvalue problem that is solved numerically. The results obtained indicates that the flow is unconditionally unstable. However, those patterns in which the RBCs concentration decreases towards the vessel walls show growth rates so small that the observability of the instability requires a very large time. Conversely, the growth rates associated to the profiles in which the RBCs concentration increases toward the vessel walls are at least three order of magnitude larger than the previous case. We therefore believe that those distributions in which the RBCs are more concentrated around the vessel center are to be considered more "stable" than those in which RBCs accumulate towards the vessel walls.

1. Introduction

A body is said inhomogeneous if the properties in the reference configuration are not uniform. The majority of bodies are inhomogeneous but when the inhomogeneity is bland they can be safely considered homogeneous. In Anand and Rajagopal (2005) the authors have shown how inhomogeneous fluids with properties that vary mildly about the mean value may lead to differences in the response which can be larger than one order of magnitude, proving that approximating a fluid as homogeneous with average properties may lead to significant errors in the computation of quantities associated with the flow.

Blood is a paradigm of an inhomogeneous complex fluid. It can be modelled as a suspension of Red Blood Cells (RBCs) in a liquid (plasma). When blood flows in "small" vessels, the RBCs volume fraction (hematocrit ϕ) varies on the cross section (Moyers-Gonzalez et al., 2008), Secomb (2017). The inhomogeneity is due to the non uniform distribution of RBCs in the cross section and it is known that in vessels with diameter less than 300 μm the RBCs do not distribute uniformly on cross section, but tend to accumulate along the axis forming a cell-free layer near the wall (Haynes, 1960). This phenomenon has been linked to the well known Fåhræus-Lindqvist effect, which describes how the viscosity of blood changes with the diameter of the vessel (see Ascolese et al., 2019; Chebbi, 2015; Copley, 1960; Fahraeus and Lindqvist, 1931; Fournier, 2012; Secomb, 2017; Secomb and Pries, 2013 and the numerous references therein reported).

Since the blood rheology depends on the hematocrit ϕ, the rheological properties are not uniform if ϕ is not spatially uniform and the flow is inhomogeneous. Such an inhomogeneity does not affect blood density[1] ρ^* (density changes due to hematocrit fluctuations are negligible) but may have significant influence on the viscous stress. Consequently, the inhomogeneity can modify the properties of the flow by triggering instabilities, so that some patterns are stable while others are not.

In this study we investigate the linear stability of a unidirectional flow in a channel of a fluid whose viscosity depends upon the hematocrit. In particular, we consider the following constitutive equation

$$\mathbb{T}^* = -p^*\mathbb{I} + 2\mu^*(\phi)\mathbb{D}^*, \tag{1}$$

where p^* and $\mathbb{D}^*$ are the pressure and the shear rate, respectively, and where the viscosity μ^* is a positive function of the hematocrit ϕ. When ϕ is uniform on the cross-section we recover the constitutive response of a Newtonian fluid. Conversely, when the hematocrit is not uniform on the vessel cross-section, the flow is inhomogeneous.

The dynamics of the hematocrit is governed by a simple advection equation in which any diffusive flux is ignored. In the framework of non-colloidal suspensions (the characteristic diameter of a RBC is sufficiently large for Brownian effects to be negligible), the solid-fluid interaction term depends on the Darcy's number (Drew and Passman, 1999; Rajagopal and Tao, 1995), which can become quite large being proportional to the square of the ratio between the macroscopic length scale and the particles size. Hence, for low Reynolds number, the two phases

* Corresponding author.
E-mail address: angiolo.farina@unifi.it (A. Farina).

[1] Starred quantities are dimensional.

https://doi.org/10.1016/j.apples.2020.100002
Received 18 April 2020; Received in revised form 10 May 2020; Accepted 13 May 2020
Available online 15 June 2020

have practically the same velocity and the suspension can be considered as a single non-homogeneous fluid (Anand and Rajagopal, 2005; Fusi, 2018; Fusi et al., 2019; Massoudi and Vaidya, 2011). The dynamics of such a fluid is governed by the linear momentum equation and the continuity equation for the fluid and by the equation for ϕ, which simply reduces to the material derivative. The steady state (when attained) depends on both boundary and initial conditions. Therefore, when no information on the initial conditions is available, the equilibrium distribution of the suspended RBCs is, in fact, arbitrary to some extent. In other words, any sufficiently regular hematocrit profile depending only on the transversal coordinate generates a flow that satisfies the motion equation (we shall resume this issue in Section 2). One therefore needs a criterion, based on reasonable physical assumptions, to select the concentration profile of the suspended particles. Hence, in order to get some insights on the possible blood flow configurations at the level of microcirculation, a stability analysis is mandatory and this is the aim of this paper.

More specifically, the objective and novelty of this study is twofold. First, to investigate the stability properties of flows, at low Reynolds number, in which the hematocrit profile ϕ depends only on the transversal coordinate, i.e. stratified flows. In particular, we consider two classes of profiles: ϕ monotonically increasing with the transversal coordinate and ϕ monotonically decreasing. The second objective is to provide further insight into the role of $\mu^*(\phi)$. We consider flows at low Reynolds number because our main focus is microcirculation: arteries terminal branches, arterioles and venules, i.e. vessels whose diameter is $0.1 - 0.6\ mm$, in which the RBCs do not distribute uniformly on cross section (Chandran et al., 2007; Cooney, 1976).

To date, relevant studies concerning stratified flows are the ones on the so-called core annular flow, i.e., parallel flow of two or more fluids with different viscosities (blood flow in a microvessel with regard to the Fåhr æus-Lindqvist effect is considered exploiting a two layer model). Hickox (1971) has studied the stability of this axisymmetric flow setting including the effects of gravity and capillary forces acting on the interface between the two liquids. He has shown that the steady Poiseuille flow of two immiscible fluids with different viscosity is unstable when the less viscous one is centrally located. Moreover, in Preziosi et al. (1989) the authors have studied the linear stability of the same base flow more extensively by varying the viscosities, the volume ratios of the two fluids, the Reynolds, etc. They have proved that the flow is generally unstable, except when the annular region is occupied by the less viscous fluid, it is sufficiently thin and the Reynolds number varies within a limited range which depends on the fluid parameters. Additional references on the stability of stratified flows under more stringent limitations of the parameters can be found in Joseph and Renardy (1993), Kouris and Tsamopoulos (2001) and Kouris and Tsamopoulos (2002).

Concerning the constitutive model (1), we recall that blood is a non-Newtonian fluid. The deviation from the classical Newtonian behavior is manifested in its yield limit, shear-thinning and stress relaxation properties (Fasano and Sequeira, 2017; Fusi et al., 2014; Yeleswarapu et al., 1998). For instance, many experiments show that for laminar flow in straight and uniform tubes, the velocity profile is blunted near the central axis, with the non-Newtonian features being strictly related to the vessel size and to the flow regime, see Liepsch (1986). Here we consider regimes where the non-Newtonian effects can be neglected to a certain extent.

The constitutive model for non-Brownian particles suspensions is much more complex than (1). Considering, for instance, the single-phase limit of the continuum model for incompressible fluid-saturated granular flows, we observe that the momentum equation has the additional term $\Gamma\nabla\phi\otimes\nabla\phi$, where the parameter Γ is referred to as the configuration stress coefficient, see Papalexandris (2004), Varsakelis and Papalexandris (2011). Furthermore, also the particles deformability should be taken into account when modeling blood. Indeed, for Stokes flow of suspensions in tubes, the non-stiffness of the particles seems to affect greatly the flow pattern, (Goldsmith and Marlow, 1979). For instance, Moyers-Gonzalez and Owens (2010) have described the steady Poiseuille flow of blood in a small tube using a two-layer fluid consisting of an outer annulus filled with plasma and an inner core where the blood is treated as a suspension of rouleaux of various sizes represented by deformable dumbbells, (Moyers-Gonzalez et al., 2008). Accordingly, the total stress is viscoelastic being composed of the small Newtonian-like contribution form the plasma and the elastic-like contribution from the RBCs. Such an approach has been used in Dimakopoulos et al. (2015) for simulating the blood flow in a stenotic vessel.

In blood flow the RBC elastic properties play an important role in the collective dynamics resulting in a nonuniform cell density on the vessel cross section (Coupier et al., 2008; Doddi and Bagchi, 2009). However, it is a well known phenomenon that, in certain flow regimes, the particles distribution in rigid spheres suspensions is not uniform on the section (Drew, 1986; Graham et al., 1991; Karnis et al., 1966). That was experimentally studied in the pioneering work by Segré and Sileberger (1962) and in the subsequent works by Nott and Brady (1994). Indeed, a general mechanistic understanding of the particles (rigid or non-rigid like RBCs) migration away from the walls has proved elusive. And also other phenomena, like the interaction between RBCs and the cells of the vessel endothelium (Secomb et al., 2001a; 2001b) and the viscoelastic properties of the plasma (Brust et al., 2013), seem influence the formation of a RBCs depleteted layer close to the vessel walls.

Concerning the evolution equation for ϕ, many approaches are possible. For instance, some authors consider the blood as a monomodal suspension of plasma and RBCs, in which a diffusive processes, driven by the shear, may occur, see Mansour et al. (2010) and Chebbi (2018). According to such an approach, the net flux of particles consists of two contributions: a diffusive flux driven by the gradient of the shear rate and a diffusive flux due to the concentration gradient (with a diffusivity proportional to the local shear rate), (Leighton and Acrivos, 1987; Phillips et al., 1992). This model has been used to predict the formation of a region close to the wall relatively poor in particles, which acts as a lubricant layer accelerating the movement of the whole suspension. In the same spirit, using scaling arguments, Leighton and Acrivos (1987) and Pranay et al. (2012), have showed that the net RBCs flux is driven by a concentration gradient whose diffusivity is proportional to the shear rate, to the local hematocrit and to the typical particle dimension. However, as pointed out in Phillips et al. (1992), such a model predicts that in a steady Couette, or Poiseuille, flow the particles volume fraction, i.e. ϕ, attains a cusp at the centerline (never observed in experiments performed on suspensions) where it takes its maximum admissible value. Such a drawback is absent in particle-migration models in which the solid-volume fraction advection-diffusion equation contains a driving term (e.g. proportional to the difference between the pressure and the integranular stress). Models of this kind have been recently developed by Monsorno et al. (2016), Monsorno et al. (2017), Lecampion and Garagash (2014), Boyer et al. (2011), and Ahnert et al. (2019) and applied to confined pressure-driven laminar flow of neutrally buoyant non-Brownian suspensions. Essentially they treat the suspension as a mixture getting mathematical problems that are characterized by considerable difficulties due to the boundary conditions, (Rajagopal and Tao, 1995). Indeed, one of the thorny issues occurring when it comes to putting mixture theory in practice, is the inability to prescribe boundary conditions for stress boundary value problems, since we do not know how to distribute the traction (or compression) among the various mixture components.

In conclusion, we can state that model (1) applies to flow regimes in which the non-Newtonian effects and the RBCs deformability play a minor role. Adopting such an approach, we are able to obtain explicit expressions for both steady velocity and pressure in a unidirectional channel flow.

To keep our analysis as general as possible, we consider four empirical laws linking the blood viscosity to the hematocrit (see equations (15)–(19)) and we find, for each of them, the basic velocity field cor-

responding to a given hematocrit transversal profile. In particular, we consider two cases that ideally represent the two main hematocrit profiles: ϕ increasing toward the vessel walls and ϕ decreasing toward the vessel walls. Then, following the classical modal analysis of infinitesimal perturbations, we add to the basic flow a "small" perturbation and investigate the linear stability. The employment of a classical normal-mode analysis results in a fourth-order eigenvalue problem that is solved numerically via a Chebyshev polynomial method.

The paper develops as follows. In Section 2 we formulate the model considering a flow between parallel plates driven by a known pressure gradient. We discard the cylindrical geometry, although physically more significant, because more involved from the numerical point of view. Similarly we do not considered a drag motion (Couette without pressure gradient) because is less indicated in the case of blood flow. In Section 3 we illustrate the linear stability analysis while Section 4 is devoted to the numerical methodology employed to solve the resulting eigenvalue problem and to the discussion of the results. Finally, in Section 5 we draw some final remarks.

2. The basic flow

We consider a mechanically incompressible flow in a channel of length L^* and amplitude $2H^*$, driven by a prescribed pressure gradient G^*. We denote by

$$\boldsymbol{v}^* = u^* \boldsymbol{e}_x + v^* \boldsymbol{e}_y \tag{2}$$

the velocity field and we introduce the viscosity $\mu^*(\phi) = \mu_p^* \mu(\phi)$, where μ_p^* is a reference viscosity and $\mu(\phi)$ is dimensionless. When the Cauchy stress is given by (1), the mathematical formulation of the problem is

$$\frac{\partial \phi}{\partial t^*} + \boldsymbol{v}^* \cdot \nabla^* \phi = 0, \tag{3}$$

$$\nabla^* \cdot \boldsymbol{v}^* = 0, \tag{4}$$

$$\rho^* \left(\frac{\partial \boldsymbol{v}^*}{\partial t^*} + \left(\boldsymbol{v}^* \cdot \nabla^* \right) \boldsymbol{v}^* \right) = -\nabla^* p^* + \mu_p^* \nabla^* \cdot \left(2\mu(\phi) \mathbb{D}^* \right), \tag{5}$$

where ρ^* is the constant and uniform fluid density.Eq. (3) is a simple advection equation since in the framework of non-colloidal suspensions the solid-fluid interaction, which would introduce in the equation a diffusive term, depends on the inverse of Darcy's number (Boyer et al., 2011; Drew and Passman, 1999), which in our case is negligible.

We rescale the problem with

$$x = \frac{x^*}{L^*}, \quad y = \frac{y^*}{L^*}, \quad H = \frac{H^*}{L^*}, \quad u = \frac{u^*}{U^*}, \quad v = \frac{v^*}{U^*}, \quad p = \frac{p^*}{\rho^* U^{*2}}, \quad G = \frac{G^* L^*}{\rho^* U^{*2}},$$

where U^* is the characteristic velocity, still to be selected. The system (3)–(5) becomes

$$\begin{cases} \dfrac{\partial \phi}{\partial t} + \boldsymbol{v} \cdot \nabla \phi = 0, \\ \nabla \cdot \boldsymbol{v} = 0, \\ \mathsf{Re}\left(\dfrac{\partial \boldsymbol{v}}{\partial t} + (\boldsymbol{v} \cdot \nabla) \boldsymbol{v} \right) = -\mathsf{Re} \nabla p + \nabla \cdot (2\mu(\phi) \mathbb{D}). \end{cases} \tag{6}$$

where $\mathsf{Re} = (\rho^* L^* U^* / \mu_p^*)$ is the Reynolds number. In particular, we take $\mathsf{Re} \lesssim \mathcal{O}(1)$, which is the typical order of magnitude for Blood flow in arterioles or venules (Fasano and Sequeira, 2017). We then look for a basic flow of the type

$$u = u_b(y), \quad v = 0, \quad p = p_b(x), \quad \phi = \phi_b(y),$$

satisfying the boundary conditions

$$u_b(H) = 0, \quad \frac{\partial u_b}{\partial y}(0) = 0, \quad p_b(0) = p_{in}, \quad p_b(1) = p_{in} - G, \tag{7}$$

where p_{in} is the dimensionless inlet pressure.

We recall that the hematocrit ϕ_b varies locally, affecting the viscous stress (but not the fluid density). In particular, since ϕ_b depends only on y and the basic velocity has no transversal component, Eq. $(6)_1$ is automatically fulfilled. This is indeed a stratified incompressible fluid where the hematocrit is constant along each particle's path. We therefore assume that $\phi_b(y)$ is a prescribed function, symmetric with respect to $y = 0$. This is a critical assumption that allows one to treat the flow in the channel – where new fluid is continuously supplied from the inlet – using an Eulerian framework (Málek and Rajagopal, 2006).

The basic flow in the upper part of the channel (in the lower part is symmetric) is the following

$$u_b(y) = \mathsf{Re}\, G \int_y^H \frac{\xi}{\mu_b(\xi)} d\xi, \tag{8}$$

$$v_b \equiv 0, \tag{9}$$

$$p_b(x) = -Gx + p_{in}, \tag{10}$$

where we set

$$\mu_b(y) = \mu\big(\phi_b(y)\big). \tag{11}$$

So far we have not specified the characteristic velocity U^*. If we take

$$U^* = \frac{G^*}{\mu_p^*} \int_0^{H^*} \frac{\xi^*}{\mu_b(\xi^*)} d\xi^*, \tag{12}$$

then

$$1 = \mathsf{Re}\, G \int_0^H \frac{\xi}{\mu_b(\xi)} d\xi, \tag{13}$$

and so

$$u_b(y) = 1 - \frac{\int_0^y \frac{\xi}{\mu_b(\xi)} d\xi}{\int_0^H \frac{\xi}{\mu_b(\xi)} d\xi}. \tag{14}$$

When $\mu_b = 1$ (Newtonian case) we get the classical parabolic profile

$$u_b(y) = 1 - \left(\frac{y}{H} \right)^2.$$

In the literature there are numerous empirical formulas relating the viscosity to the hematocrit (see, for instance, Whitmore (1968), Fournier (2012) and Bayliss (1952) Chapter 6 and the recent review (Hund et al., 2017)). All these formulas are characterized by the fact that μ_b is an increasing function of ϕ. We consider here a list of the most common expressions found in the literature (Cokelet, 1963; Hatschek, 1920; Nubar, 1967):

$$\mu(\phi) = \frac{1}{1 - g(\phi, T)\phi} \text{ (Charm and Kurland, [8])} \tag{15}$$

with

$$g(\phi, T) = c_o \exp\left\{ c_1 \phi + \left(\frac{c_2}{T} \right) \exp(-c_3 \phi) \right\}, \tag{16}$$

$$\mu(\phi) = \frac{1}{1 - (\phi)^{1/3}}, \text{ (Hatschek, 1920)}, \tag{17}$$

$$\mu(\phi) = \frac{1}{(1 - \phi)^{2.5}}, \text{ (Cokelet, 1963)}, \tag{18}$$

$$\mu(\phi) = \frac{0.75}{0.75 - \phi}, \text{ (Nubar, 1967)}. \tag{19}$$

The plots in Fig. 1 show the viscosity as a function of the hematocrit for the expressions (15)–(19), while the plots in Fig. 2 show the corresponding velocity profiles obtained from (14) when the hematocrit distribution on the cross-section is

$$\phi(y) = \frac{\phi_M \phi_m}{(1 - y^2)\phi_m + y^2 \phi_M}. \tag{20}$$

In (20) $\phi_m = 0.2$, $\phi_M = 0.7$ are the minimum and maximum values attained by the hematocrit. Such a choice of $\phi_b(y)$ does not reflect any real situation but it provides a regular symmetric function bounded between two reasonable values of the hematocrit attaining the maximum at $y = 0$. As one can notice, the basic velocities related to the various empirical expression of the viscosity are very similar.

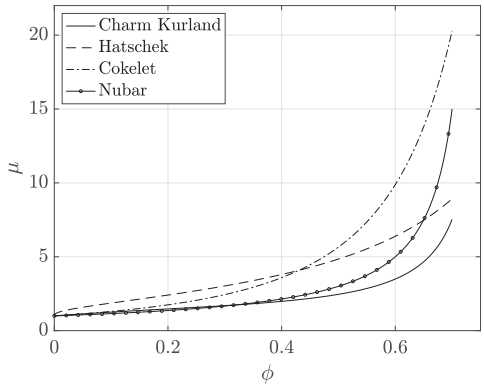

Fig. 1. Examples of $\mu(\phi)$.

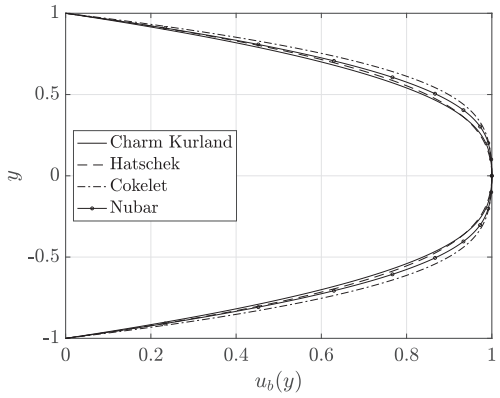

Fig. 2. Corresponding velocity profiles.

3. Two dimensional perturbation

To perform a linear stability analysis of the basic flow (14), we consider the following perturbed solution

$$u(x,y,t) = u_b(y) + \hat{u}(y)e^{i(\alpha x-\omega t)}, \tag{21}$$

$$v(x,y,t) = \hat{v}(y)e^{i(\alpha x-\omega t)}, \tag{22}$$

$$p(x,y,t) = p_b(x) + \hat{p}(y)e^{i(\alpha x-\omega t)}, \tag{23}$$

$$\phi(x,y,t) = \phi_b(y) + \hat{\phi}(y)e^{i(\alpha x-\omega t)}, \tag{24}$$

where $|\hat{\ }| \ll 1$, $\alpha \in \mathbb{R}$ is the wave number and $\omega \in \mathbb{C}$ is the frequency. Introducing

$$c = \frac{\omega}{\alpha}, \quad \text{with} \quad c \in \mathbb{C}, \tag{25}$$

the perturbation phase can be rewritten as

$$i(\alpha x - \omega t) = i\alpha(x - ct).$$

Setting

$$\left.\frac{d\mu(\phi)}{d\phi}\right|_{\phi=\phi_b(y)} = \dot{\mu}_b(y), \tag{26}$$

we consider an expansion of the viscosity function up to the linear term, that is

$$\mu(\phi(x,y,t)) = \mu_b(y) + \dot{\mu}_b(y)\,\hat{\phi}(y)e^{i(\alpha x-\omega t)}, \tag{27}$$

Inserting (21)–(24) in $(6)_1$ and $(6)_2$ and disregarding nonlinear terms we find

$$i(\alpha u_b - \omega)\hat{\phi} + \hat{v}\phi_b' = 0, \tag{28}$$

$$\hat{v}' + i\alpha\hat{u} = 0, \tag{29}$$

where

$$(\,\cdot\,)' = \frac{d(\,\cdot\,)}{dy}.$$

Inserting (21)–(24) and (27) in $(6)_3$ we obtain

$$\begin{aligned}\mathrm{Re}\left(-i\omega\hat{u} + i\alpha u_b\hat{u} + u_b'\hat{v}\right) &= -i\alpha\mathrm{Re}\,\hat{p} \\ &+ -2\alpha^2\mu_b\hat{u} + \frac{d}{dy}\left[\mu_b(\hat{u}' + i\alpha\hat{v}) + \dot{\mu}_b\,\hat{\phi}u_b'\right]\end{aligned} \tag{30}$$

$$\begin{aligned}\mathrm{Re}\left(-i\omega\hat{v} + i\alpha u_b\hat{v}\right) &= -\mathrm{Re}\,\hat{p}' \\ &+ i\alpha\left(\mu_b(\hat{u}' + i\alpha\hat{v}) + \dot{\mu}_b\,\hat{\phi}u_b'\right) + \frac{d}{dy}\left[2\mu_b\hat{v}'\right]\end{aligned} \tag{31}$$

Exploiting (29) and introducing

$$Q(y) = \mu_b(y) - 1,$$

$$P(y) = \dot{\mu}_b(y)\phi_b'(y)u_b'(y),$$

Eqs. (30) and (31) can be rewritten as

$$\begin{aligned}\mathrm{Re}\left(-i\omega\hat{u} + i\alpha u_b\hat{u} + u_b'\hat{v}\right) &= -i\alpha\mathrm{Re}\,\hat{p} - 2\alpha^2 Q\hat{u} \\ &+ \left(\frac{d^2}{dy^2} - \alpha^2\right)\hat{u} + \frac{d}{dy}\left[Q(\hat{u}' + i\alpha\hat{v}) + P\frac{\hat{\phi}}{\phi_b'}\right],\end{aligned} \tag{32}$$

$$\begin{aligned}\mathrm{Re}\left(-i\omega\hat{v} + i\alpha u_b\hat{v}\right) &= -\mathrm{Re}\,\hat{p}' + \left(\frac{d^2}{dy^2} - \alpha^2\right)\hat{v} \\ &+ i\alpha\left[Q(\hat{u}' + i\alpha\hat{v}) + P\frac{\hat{\phi}}{\phi_b'}\right] + \frac{d}{dy}\left[2Q\hat{v}'\right]\end{aligned} \tag{33}$$

On eliminating the pressure between (32) and (33) and exploiting (29), we get

$$\begin{aligned}\mathrm{Re}\left[i(\alpha u_b - \omega)(\hat{u}' - i\alpha\hat{v}) + u_b''\hat{v}\right] &= \left(\frac{d^2}{dy^2} - \alpha^2\right)(\hat{u}' - i\alpha\hat{v}) \\ &+ \left(\frac{d^2}{dy^2} + \alpha^2\right)\left[Q(\hat{u}' + i\alpha\hat{v}) + P\frac{\hat{\phi}}{\phi_b'}\right] - 2i\alpha\frac{d}{dy}\left[Q(\hat{v}' - i\alpha\hat{u})\right].\end{aligned} \tag{34}$$

If we now introduce the new variable $f(y)$

$$\hat{\phi} = \phi_b'\,f,$$

implying that $\hat{\phi}$ is symmetric with respect to $y = 0$, Eqs. (28) and (29) can be rewritten as

$$\hat{v} = i\alpha(c - u_b)f, \qquad \hat{u} = -\frac{d}{dy}\left[(c - u_b)f\right].$$

On substituting the above into (34) we get the fourth order eigenvalue problem

$$\begin{aligned}i\alpha\mathrm{Re}\left\{(u_b - c)(\mathrm{D}^2 - \alpha^2) - u_b''\right\}\left[(u_b - c)f\right] &= (\mathrm{D}^2 - \alpha^2)^2\left[(u_b - c)f\right] \\ &+ (\mathrm{D}^2 + \alpha^2)\left\{Q(\mathrm{D}^2 + \alpha^2)\left[(u_b - c)f\right] + Pf\right\} - 4\alpha^2\mathrm{D}\left\{Q\mathrm{D}\left[(u_b - c)f\right]\right\},\end{aligned} \tag{35}$$

where

$$\mathrm{D}^k = \frac{d^k}{dy^k}$$

and whose boundary conditions are

$$f|_{\pm H} = 0, \quad f'|_{\pm H} = 0. \tag{36}$$

System (35) and (36) provides the eigenvalues $c \in \mathbb{C}$, and the relative eigenfunctions f, that allows one to establish if the basic flow (8)–(10), corresponding to the prescribed ϕ_b and to the selected $\mu_b(\phi)$, is linearly stable or not. In particular, when $Im(c) > 0$ the system is unstable.

Remark 1. We observe that when $Q = P = 0$, i.e. when $\mu = 1$, setting $g = (u_b - c)f$ we recover the classical Orr-Sommerfeld equation

$$i\alpha \mathsf{Re}\left\{(u_b - c)(\mathsf{D}^2 - \alpha^2) - u_b''\right\} g = (\mathsf{D}^2 - \alpha^2)^2 g.$$

Eq. (35) can be rewritten as

$$\mathcal{L}_0 f + c\mathcal{L}_1 f + c^2 \mathcal{L}_2 f = 0,$$

where $\mathcal{L}_j$ are the differential operators

$$\mathcal{L}_j = \sum_{k=0}^{4} L_{jk}(y)\mathsf{D}^k. \tag{37}$$

The coefficients $L_{jk}(y)$, which are reported in Appendix A, are evaluated through the symbolic software MAXIMA, Maxima.sourceforge.net (2011). Following Varsakelis and Papalexandris (2015), we state that the spectrum of (37) is purely discrete. The proof of this result can be obtained extending the proof of Lin (1961), developed for the classical Orr-Sommerfeld equation.

4. Numerical solution

This section is devoted to the numerical solution of the problem (35) and (36). Our main goal is to determine the eigenvalue with the largest imaginary part as a function of the wave number α and for a fixed value of the Reynolds number Re. Therefore we set

$$\sigma = \max_{c \in \Sigma} Im(c),$$

where Σ is the spectrum of system (35) and (36). For fixed Re, we find that σ is a function of the wave number α, i.e. $\sigma = \sigma(\alpha)$. For simplicity we assume that the length of the channel and the semi-amplitude of the channel are equal so that $H = 1$ and the channel walls are $y = \pm 1$.

Concerning the hematocrit profile $\phi_b(y)$, we select

$$\phi_b(y) = Cy^2 + d, \tag{38}$$

where $d \in [0, 1]$ and $-d \leqslant C \leqslant 1 - d$, so that $\phi_b(y) \in [0, 1]$ when $y \in [-1, 1]$. In particular, we consider two cases:

1. $C > 0$, the hematocrit is larger at the channel walls and so is the viscosity (which is an increasing function of the hematocrit).
2. $C < 0$, the RBCs concentration is larger in the middle of the channel and so is viscosity.

Of course other choices of $\phi_b(y)$ different from (38) are possible. Here we make use of (38) because of its simple form (it is an even continuously differentiable function) and because it allows, by simply changing the sign of the constant C, to represent the two most important cases: increasing/decreasing hematocrit with y.

Eq. (35) is discretized approximating the differential operators via a pseudo-spectral collocation method. The functions are evaluated using Chebyshev interpolation and the discretized generalized problem is solved through a QR decomposition in which spurious, i.e. unphysical, eigenvalues are ruled out by comparing results on grids of different size. The adopted procedure in implemented in Matlab® exploiting the well known CHEBYFUN package (Driscoll et al., 2014; Weideman and Reddy, 2000). The robustness of the code has been tested by computing the eigenvalues of the Orr-Sommerfeld equation.

As a preliminary case we consider a simple linear model for μ_b

$$\mu_b(\phi) = A\phi + 1, \quad \text{with} \quad A > 0, \tag{39}$$

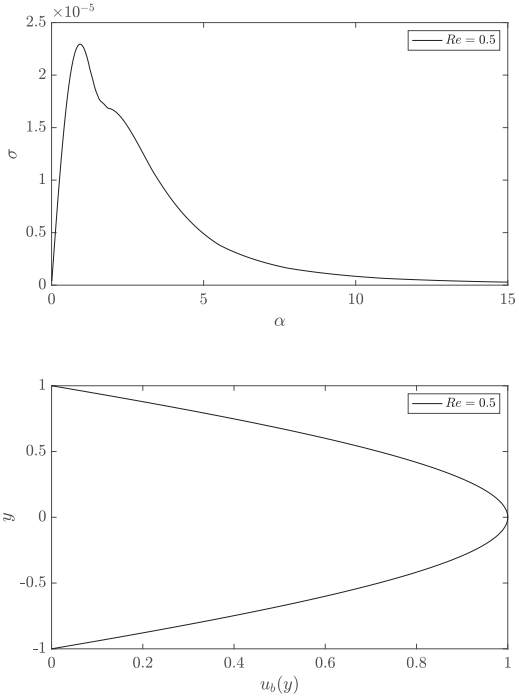

Fig. 3. $A = 0.5$, $C = 0.8$, $d = 10^{-2}$.

which, combined with (38), gives

$$\mu_b(y) = ACy^2 + (Ad + 1). \tag{40}$$

Exploiting (13) we can compute the explicit expression of the velocity profile

$$u_b(y) = 1 - K \ln\left(\theta y^2 + 1\right), \quad \text{with} \quad \theta = \frac{AC}{Ad + 1}, \quad \text{and} \quad K = \frac{1}{\ln\left(\theta + 1\right)}. \tag{41}$$

Model (39) and the corresponding basic flow is purely abstract and does not reflect any real situation. This notwithstanding, such a choice is quite useful because it allows one to determine explicitly the basic profile u_b and it provides a good example for studying how σ depends on the distribution of the RBCs within the channel.

In the example showed in Fig. 3 we take $A = 0.5$, $C = 0.8$, $d = 10^{-2}$, which generates a basic profile (41) not exhibiting any flex. In Fig. 4 we choose $A = 50$, $C = 0.8$, $d = 10^{-2}$, whose corresponding velocity profile (41) shows a flex. In both cases Re is 0.5 and $C > 0$, so that the RBCs distribution increases as y approaches the lateral walls. The quantity σ is positive for every value of α, showing that the perturbed flow is unconditionally unstable but different order of magnitude of σ are obtained depending on the value of A. In particular, we notice that for $A = 0.5$, $\sigma \approx 10^{-5}$ (corresponding to a wave number $\alpha \approx 1$) so that the instability develops very slowly. On the other hand, when $A = 50$, i.e. when the viscosity is two order of magnitude larger than the previous case, we get a maximum $\sigma \approx 10^{-3}$ and the instability develops two orders of magnitude faster. We observe that this result is in accordance with what found in Varsakelis and Papalexandris (2015). We now look at the second case, i.e. $C < 0$, the RBCs distribution decreases as y approaches the lateral walls (a pattern considered physically consistent according to the classical literature (Haynes, 1960; Secomb, 2017). In Fig. 5 we take $A = 0.5$, $C = -0.2$, $d = 0.5$, while in Fig. 6 we take $A = 50$, $C = -0.2$, $d = 0.5$, and in both cases Re = 0.5. Differently from the case in which $C > 0$, now the basic velocity profiles do not exhibit any flex point. The maximum σ is $\mathcal{O}(10^{-5})$ for $A = 0.5$, while for $A = 50$ the maximum is $\mathcal{O}(10^{-6})$. This behavior seems to indicate that a large variation of the viscosity has a stabilizing effect on the perturbed flow. Indeed, looking at Fig. 6 we observe that when the basic viscosity $\mu_b(y)$ is increased of

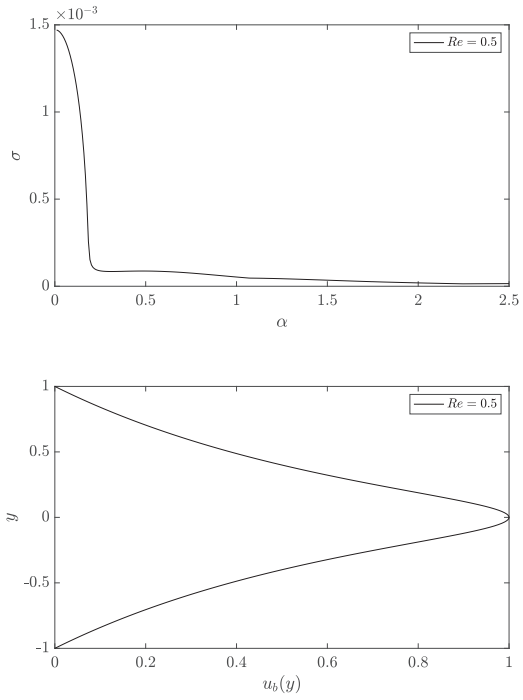

Fig. 4. $A = 50$, $C = 0.8$, $d = 10^{-2}$.

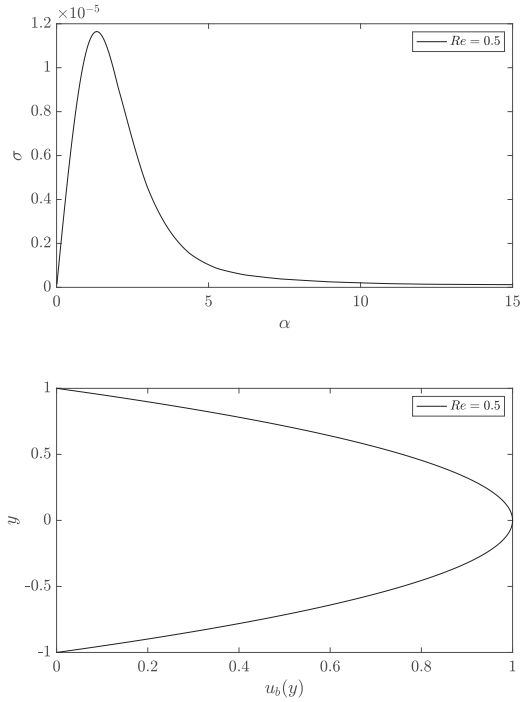

Fig. 5. $A = 0.5$, $C = -0.2$, $d = 0.5$.

two order of magnitude, the maximum eigenvalue σ is reduced by one order of magnitude. The results obtained are reported in Table 1.

Such preliminary analysis indicates the following facts:

i) The flow (39)–(41) is unconditionally unstable for "small" values of the Reynold number independently on the monotonicity of ϕ_b (increasing and decreasing).
ii) The patterns in which the RBCs are concentrated in the central part of the channel (case 2) are "less unstable" than the ones in which the RBCs are concentrated close to the walls (case 1).

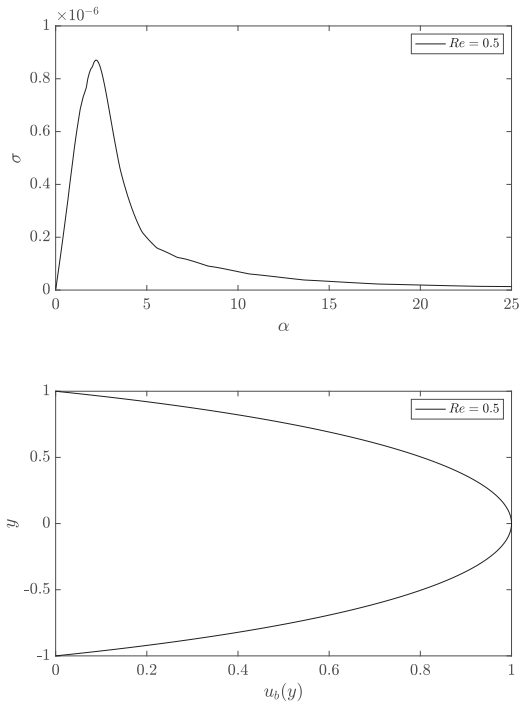

Fig. 6. $A = 50$, $C = -0.2$, $d = 0.5$.

Table 1
Summary of results related to the flow (39)–(41).

C	A	σ	C	A	σ
0.8	0.5	$\mathcal{O}(10^{-5})$	−0.2	0.5	$\mathcal{O}(10^{-5})$
	50	$\mathcal{O}(10^{-3})$		50	$\mathcal{O}(10^{-6})$

iii) Case 1 and case 2 show different responses for what concerns the viscosity dependence on the hematocrit. In particular, in case 1 the instability develops slowly when the viscosity depends "weakly" on ϕ. Indeed when $A = 0.5$ we have $\sigma \approx 10^{-5}$, while for $A = 50$ we get $\sigma \approx 10^{-3}$. Case 2 is characterized by a completely opposite behavior.

Let us now focus on the Charm and Kurland empirical relation (15) where the hematocrit ϕ and the plasma viscosity μ are linked by a nonlinear relation. We take $T = 310\,^oK$, $c_o = 0.07$, $c_1 = 2.49$, $c_2 = 1107\,^oK$ and $c_3 = 1.49$ (see Charm and Kurland (1974)). The basic distribution $\phi_b(y)$ is still given by (38).

We plot σ as a function of α and we plot the basic velocity profile, the Reynolds number being always equal to 0.5. In Fig. 7 we take $C = 0.4$, $d = 10^{-2}$ and the basic profile $u_b(y)$ does not show a flex point. In Fig. 8 we set $C = 0.75$, $d = 10^{-2}$ and $u_b(y)$ shows a flex. The constant C is positive meaning that we are in case 1. The quantity σ is positive for every value of α also in this case, so that the perturbed flow is unconditionally unstable but different orders of magnitude of σ are obtained depending on the value of C. In particular we notice that for $C = 0.4$ the maximum value of σ is $\sigma \approx 10^{-5}$, while for $C = 0.75$ the maximum of σ is of the order of 10^{-3}, i.e. two orders of magnitude smaller. This means that with lower values of the hematocrit the system develops the instability slower than for larger values of the hematocrit, in accordance with the case in which the viscosity is given by (40). We then focus on case 2, taking $C < 0$ (larger hematocrit in the center of the channel). In the plots displayed in Fig. 9 we take $C = -0.45$, $d = 0.5$, while in Fig. 10 we take $C = -0.01$, $d = 0.5$. Looking at Figs. 9 and 10 we notice an interesting feature: a reduction of the steepness $|C|$ of the RBCs distribution results in a reduction of the maximum growth rate σ. In practice, the smaller is the gradient of the hematocrit, the "less unstable" is the fluid.

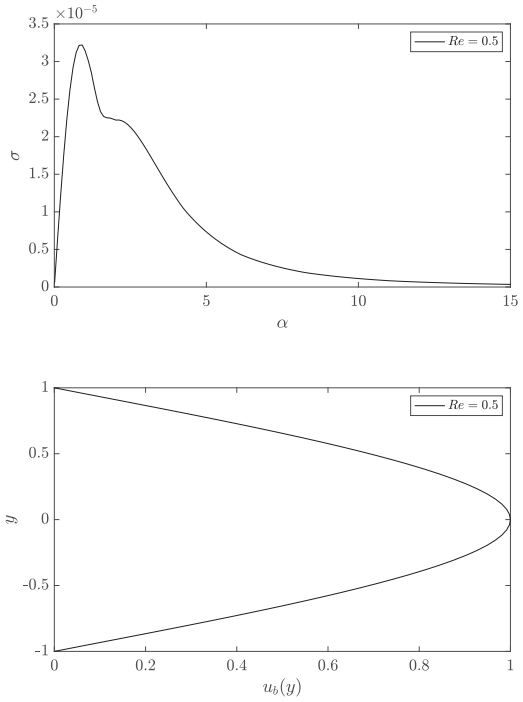

Fig. 7. $C = 0.4$, $d = 10^{-2}$.

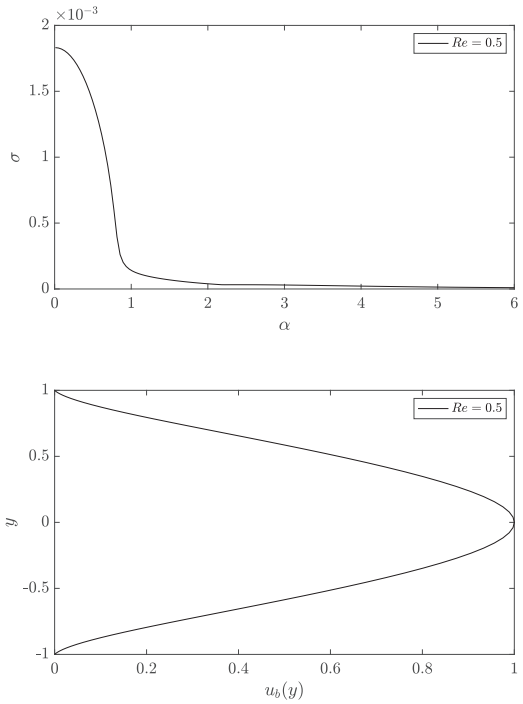

Fig. 8. $C = 0.75$, $d = 10^{-2}$.

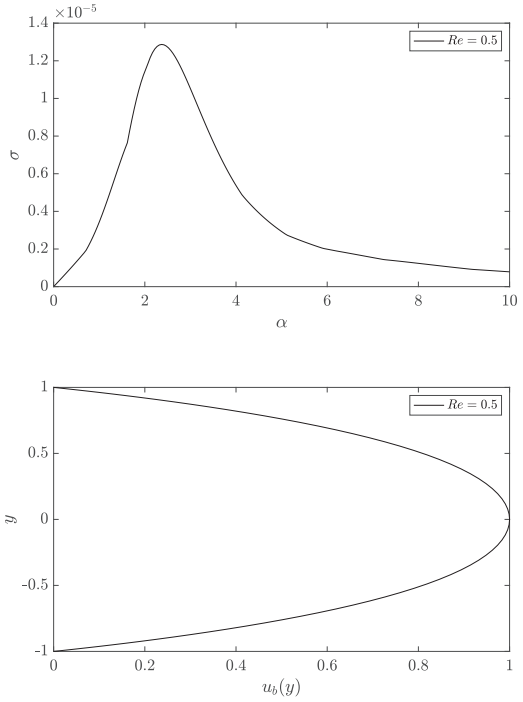

Fig. 9. $C = -0.45$, $d = 0.5$.

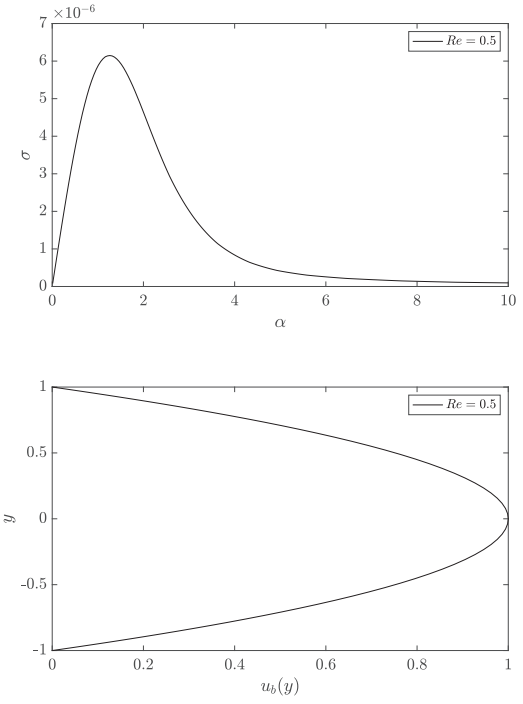

Fig. 10. $C = -0.01$, $d = 0.5$.

Indeed, for $C = -0.01$ (which means an almost flat profile of $\phi_b(y)$) the maximum rate σ is $O(10^{-6})$, while for $C = -0.45$ the maximum rate σ is $O(10^{-5})$.

When considering the empirical expressions for the viscosity (17)–(19) we obtain results very similar to the Charm-Kurland case. Therefore, we do no show the plots of $\sigma(\alpha)$, since they are essentially equal to the ones Figs. 7–10.

5. Conclusion

In this study we investigate the stability of a unidirectional plane Poiseuille blood flow modeled as a inhomogeneous fluid whose viscosity depends on the hematocrit. We consider two types of basic flow: one in which the hematocrit grows from the central axis to the wall of the vessel (case 1) and one in which the hematocrit has the opposite behavior (case 2). For each case we consider four different empirical laws linking the blood viscosity to the hematocrit.

By exploiting a classical normal-mode analysis, the stability of the system is studied solving a numerical polynomial eigenvalue problem. According to our simulations the flows of interest are unconditionally unstable for $\mathrm{Re} \lesssim \mathcal{O}(1)$, both in case 1 and case 2 and for all the rheological models considered. However, even though the flow is predicted to be unconditionally unstable, the growth rates related to case 1 and 2 are considerably different. We can indeed say, with some confidence, that case 1 is "more" unstable than case 2, meaning that the time required for the development of the instability in case 1 is at least a couple of orders of magnitude smaller than the one of case 2.

The laws expressing the blood viscosity in terms of the hematocrit produce different effects depending on which situation we are considering (case 1 and case 2). As for case 1, we remark that the more pronounced is the dependence of the viscosity on ϕ, the shorter is the time in which the instability occurs. In case 2 the opposite behavior is observed: a strong dependence of the viscosity on the hematocrit causes a "stabilization" of the flow, meaning that the perturbations growth rate is shorter when the viscosity in the inner part is one order of magnitude larger than the one of the marginal layer.

The stability analysis carried out in this paper constitutes the first step towards understanding the role of the hematocrit distribution for spatially inhomogeneous blood flows occurring in microvessels. However, given the complex rheology of blood due to non-Newtonian effects and cells defomrability (phenomena disregarded in this study), the results here obtained are just physical insights towards a more complete theory and therefore closer to the physiological phenomenon. As a consequence we note that a possible development of the present study is represented by the investigation of the density changes due to hematocrit fluctuations where it is likely that a small fluid compressibility due RBCs concentration may result in a stabilizing effect. This, however, would entail the development of a constitutive model linking pressure and hematocrit, a problem that, in the authors' knowledge, has not yet been investigated.

Appendix A. Appendix

We provide here the coefficients introduced in (37)

$$\begin{aligned}
L_{00}(y) = &-Q\left(\frac{d^4u_b}{dy^4}\right) - \frac{d^4u_b}{dy^4} - 2\left(\frac{dQ}{dy}\right)\left(\frac{d^3u_b}{dy^3}\right)\\
&+ 2Q\,\alpha^2\left(\frac{d^2u_b}{dy^2}\right) + 2\alpha^2\left(\frac{d^2u_b}{dy^2}\right)\\
&- \left(\frac{d^2Q}{dy^2}\right)\left(\frac{d^2u_b}{dy^2}\right) + 2\left(\frac{dQ}{dy}\right)\alpha^2\left(\frac{du_b}{dy}\right) - i\mathrm{Re}\,\alpha^3\,{u_b}^2\\
&- Q\,\alpha^4\,u_b - \alpha^4\,u_b - \left(\frac{d^2Q}{dy^2}\right)\alpha^2\,u_b - P\,\alpha^2 - \frac{d^2P}{dy^2},\\
L_{01}(y) = &-4Q\left(\frac{d^3u_b}{dy^3}\right) - 4\left(\frac{d^3u_b}{dy^3}ub\right) - 6\left(\frac{dQ}{dy}\right)\left(\frac{d^2u_b}{dy^2}\right)\\
&+ 2i\mathrm{Re}\alpha\,ub\left(\frac{du_b}{dy}\right)\\
&+ 4Q\,\alpha^2\left(\frac{du_b}{dy}\right) + 4a^2\left(\frac{du_b}{dy}\right) - 2\left(\frac{d^2Q}{dy^2}\right)\left(\frac{du_b}{dy}\right)\\
&+ 2\left(\frac{dQ}{dy}\right)\alpha^2\,ub - 2\left(\frac{dP}{dy}\right),\\
L_{02}(y) = &-6Q\left(\frac{d^2u_b}{dy^2}\right) - 6\left(\frac{d^2u_b}{dy^2}\right) - 6\left(\frac{dQ}{dy}\right)\left(\frac{du_b}{dy}\right)\\
&+i\mathrm{Re}\alpha\,ub^2 + 2Q\,\alpha^2\,ub + 2\alpha^2\,ub - \left(\frac{d^2Q}{dy^2}\right)ub - P,\\
L_{03}(y) = &-4Q\left(\frac{du_b}{dy}\right) - 4\left(\frac{du_b}{dy}\right) - 2\left(\frac{dQ}{dy}\right)ub,\\
L_{04}(y) = &-(Q+1)u_b.
\end{aligned}$$

$$L_{10}(y) = 2i\mathrm{Re}\,\alpha^3\,ub + Q\,\alpha^4 + \alpha^4 + \left(\frac{d^2Q}{dy^2}\right)\alpha^2,$$

$$L_{11}(y) = -2i\mathrm{Re}\alpha\left(\frac{du_b}{dy}\right) - 2\left(\frac{dQ}{dy}\right)a^2,$$

$$L_{12}(y) = -2i\mathrm{Re}\alpha\,ub - 2Q\,\alpha^2 - 2\alpha^2 + \frac{d^2Q}{dy^2},$$

$$L_{13}(y) = 2\left(\frac{dQ}{dy}\right),$$

$$L_{14}(y) = Q + 1.$$

$$L_{20}(y) = -i\mathrm{Re}\alpha^3, \qquad L_{21} = 0, \qquad L_{22} = i\mathrm{Re}\alpha, \qquad L_{23} = L_{24} = 0.$$

References

Ahnert, T., Münch, A., Wagner, B., 2019. Models for the two-phase flow of concentrated suspensions. Eur. J. Appl. Math. 30, 585–617.

Anand, M., Rajagopal, K., 2005. A note on the fows of inhomogeneous fluids with shear-dependent viscosities. Arch. Mech. 57 (5), 417–428.

Ascolese, M., Farina, A., Fasano, A., 2019. The Fåhræus-Lindqvist effect in small blood vessels: how does it help the heart? J. Biol. Phys. 45, 379–394. doi:10.1007/s10867-019-09534-4.

Bayliss, L.E., 1952. Reology of blood and lymph. In: in Deformation and Flow in Biological Systems. North-Holland.

Boyer, F., Guazzelli, E., Pouliquen, O., 2011. Unifying suspension and granular rheology. Phys. Rev. Lett. 107, 188301–188306.

Brust, M., Schaefer, C., Doerr, R., Pan, L., Garcia, M., Arratia, P.E., Wagner, C., 2013. Rheology of human blood plasma: viscoelastic versus newtonian behavior. Phys. Rev. Lett. 110, 078305.

Chandran, K.B., Yoganathan, A.P., Rittgers, S.E., 2007. Biofluid Mechanics. The Human Circulation, CRC.

Charm, S.E., Kurland, G.S., 1974. Blood Flow and Microcirculation. John Wiley.

Chebbi, R., 2015. Dynamics of blood flow: modeling of the Fahraeus-Lindqvist effect. J. Biol. Phys. doi:10.1007/s10867-015-9376-1.

Chebbi, R., 2018. Dynamics of blood flow: modeling of Fåhraeus and Fåhraeus–Lindqvist effects using a shear-induced red blood cell migration model. J. Biol. Phys. 44, 591–603. doi:10.1007/s10867-018-9508-5.

Cokelet, G.R., 1963. The rheology of human blood. In: Doctoral Dissertation. M.I.T, Cambridge, MA.

Cooney, D.O., 1976. Biomedical engineering principles: An introduction to fluid. In: Heat and Mass Transport Processes. Marcel Dekker.

Copley, A.L., 1960. Flow Properties of Blood, stainsby g. Pergamon Press.

Coupier, G., Kaoui, B., Podgorski, T., Misbah, C., 2008. Noninertial lateral migration of vesicles in bounded poiseuille flow. Phys. Fluids 20, 111702.

Dimakopoulos, Y., Kelesidis, G., Tsouka, S., Georgiou, G.C., Tsamopoulos, J., 2015. Hemodynamics in stenotic vessels of small diameter under steady state conditions: effect of viscoelasticity and migration of red blood cells. Biorheology 52, 183–210.

Doddi, S.K., Bagchi, P., 2009. Three-dimensional computational modeling of multiple deformable cells flowing in microvessels. Phys. Rev. E 79, 046318.

Drew, D.A., 1986. Flow Structure in the Poiseuille Flow of a Particle-fluid Mixture. SIAM Workshop on Multiphase Flow, June 2–4.

Drew, D.A., Passman, S.L., 1999. Theory of multicomponent fluids. In: Applied Mathematical Sciences, Vol. 135. Springer.

Driscoll, T.A., Hale, N., Trefethen, L.N., 2014. Chebfun Guide. Pafnuty Publications, Oxford.

Fahraeus, R., Lindqvist, T., 1931. The viscosity of the blood in narrow capillary tubes. Am. J. Physiol. 96, 562–568.

Fasano, A., Sequeira, A., 2017. Hemomath. The Mathematics of Blood. Springer.

Fournier, R.L., 2012. Basic Transport Phenomena in Biomedical Engineering. CRC.

Fusi, L., 2018. Two-dimensional thin-film flow of an incompressible inhomogeneous fluid in a channel. J. Nonnewton Fluid Mech. 260, 87–100.

Fusi, L., Farina, A., Rosso, F., 2014. Retrieving the Bingham model from a bi-viscous model: some explanatory remarks. Appl. Math. Lett. 27, 11–14.

Fusi, L., Farina, A., Rosso, F., Rajagopal, K., 2019. Thin-film flow of an inhomogeneous fluid with density-dependent viscosity. Fluids 4, 30.

Goldsmith, H.L., Marlow, J.C., 1979. Flow behavior of erythrocytes. II. particle motions in concentrated suspensions of ghost cells. J. Colloid Interface Sci. 71, 383–407.

Graham, A.L., Altobelli, S.A., Fukushima, E., Mondy, L.A., Stephens, T.S., 1991. Note: NMR imaging of shear-induced diffusion and structure in concentrated suspensions undergoing couette flow. J. Rheol. 35, 191–198.

Hatschek, E., 1920. Eine reihe von abnormen liesegangschen schictung. Koll. Zeitschr 27, 225–229.

Haynes, R.F., 1960. Physical basis of the dependence of blood viscosity on tube radius. Am. J. Physiol. 198, 1193–1200.

Hickox, C.E., 1971. Instability due to viscosity and density stratification in axisymmetric pipe flow. Phys. Fluids 14, 251–262.

Hund, S.J., Kameneva, M.V., Antaki, J.F., 2017. A quasi-mechanistic mathematical representation for blood viscosity. Fluids 2, 10–36.

Joseph, D.D., Renardy, Y., 1993. Fundamentals of two-fluid dynamics. In: Part II Lubricated Transport. Springer, New York.
Karnis, A., Goldsmithand, H.L., Mason, S.G., 1966. The kinetics of flowing dispersions: I. Concentrated suspensions of rigid particles. J. Colloid Interfaces Sci. 22, 531–543.
Kouris, C., Tsamopoulos, J., 2001. Dynamics of axisymmetric core-annular flow in a straight tube: I. The more viscous fluid in the core, bamboo waves. Phys. Fluids 13, 841–858.
Kouris, C., Tsamopoulos, J., 2002. Dynamics of the axisymmetric core-annular flow. II. the less viscous fluid in the core, saw tooth waves. Phys. Fluids 13, 1011–1029.
Lecampion, B., Garagash, D.I., 2014. Confined flow of suspensions modelled by a frictional rheology. J. Fluid Mech. 759, 197–235.
Leighton, D., Acrivos, A., 1987. The shear-induced migration of particles in concentrated suspensions. J. Fluid Mech 181, 415–427.
Liepsch, D.W., 1986. Flow in tubes and arteries - a comparison. Biorheology 23, 395–402.
Lin, C.C., 1961. Some mathematical problems in the theory of the stability of parallel flows. J. Fluid Mech. 10, 430–438.
Málek, J., Rajagopal, K., 2006. On the modeling of inhomogeneous incompressible fluid–like bodies. Mech. Mater. 38 (3), 233–242.
Mansour, M.H., Bressloff, N.W., Shearman, C.P., 2010. Red blood cell migration in microvessels. Biorheology 47, 73–93. doi:10.3233/BIR-2010-0560.
Massoudi, M., Vaidya, A., 2011. Unsteady flows of inhomogeneous incompressible fluids. Int. J. Non-Linear Mech. 46, 738–741.
Maxima.sourceforge.net, 2011. Maxima, a computer algebra system, version 5.25.1. see. http://www.maxima.sourceforge.net.
Monsorno, D., Varsakelis, C., Papalexandris, M.V., 2016. A thermomechanical model for granular suspensions. J. Fluid Mech. 808, 410–440.
Monsorno, D., Varsakelis, C., Papalexandris, M.V., 2017. Poiseuille flow of dense non-colloidal suspensions: the role of intergranular and nonlocal stresses in particle migration. J. Non-Newtonian Fluid Mech. 247, 229–238.
Moyers-Gonzalez, M.A., Owens, R.G., 2010. Mathematical modelling of the cell-depleted peripheral layer in the steady flow of blood in a tube. Biorheology 47, 39–71.
Moyers-Gonzalez, M.A., Owens, R.G., Fang, J., 2008. A non-homogeneous constitutive model for human blood. Part i: model derivation and steady flow. J. Fluid Mech. 617, 327–354.
Nott, P.R., Brady, J.F., 1994. Pressure-driven flow of suspensions: simulation and theory. J. Fluid Mech. 275, 157–199.
Nubar, Y., 1967. Effect of slip on the rheology of a composite fluid: application to blood. Biorheology 4, 113–117.
Papalexandris, M.V., 2004. A two-phase model for compressible granular flows based on the theory of irreversible processes. J. Fluid Mech. 517, 103–112. doi:10.1017/S0022112004000874.
Phillips, R.J., Armstrong, R.C., Brown, R.A., 1992. A constitutive equation for concentrated suspensions that accounts for shear-induced particle migration. Phys. Fluids 4, 30–40.
Pranay, P., Henriquez-Rivera, R.G., Graham, M.D., 2012. Depletion layer formation in suspensions of elastic capsules in newtonian and viscoelastic fluids. Phys. Fluids 24, 061902.
Preziosi, L., Chen, K., Joseph, D.D., 1989. Lubricated pipelining: stability of core-annular flow. J. Fluid Mech. 201, 323–338.
Rajagopal, K.R., Tao, L., 1995. Mechanics of Mixtures. World Scientific, Singapore.
Secomb, T.W., 2017. Blood flow in the microcirculation. Annu. Rev. Fluid Mech. 49, 443–461.
Secomb, T.W., Hsu, R., Pries, A.R., 2001. Effect of the endothelial surface layer on transmission of fluid shear stress to endothelial cells. Biorheology 38, 143–150.
Secomb, T.W., Hsu, R., Pries, A.R., 2001. Motion of red blood cells in a capillary with an endothelial surface layer: effect of flow velocity. Am. J. Physiol. Heart Circ. Physiol. 281, 629–636.
Secomb, T.W., Pries, A.R., 2013. Blood viscosity in microvessels: experiment and theory. C.R. Phys. 14, 470–478.
Segré, G., Sileberger, A., 1962. Behaviour of macroscopic rigid spheres in poiseuille flow. J. Fluid Mech. 14, 115–135.
Varsakelis, C., Papalexandris, M.V., 2011. Low-mach-number asymptotics for two-phase flows of granular materials. J. Fluid Mech. 669, 472–497. doi:10.1017/S0022112010005173.
Varsakelis, C., Papalexandris, M.V., 2015. Stability analysis of Couette flows of spatially inhomogeneous complex fluids, proceedings of the royal society a: mathematical. Phys. Eng. Sci. 471. 20150529
Weideman, J.A., Reddy, S.C., 2000. A MATLAB differentiation matrix suite. ACM Trans. Math. Softw. 26, 465–519.
Whitmore, R.L., 1968. Rheology of Circulation. Pergamon Press.
Yeleswarapu, K.K., Kameneva, M.V., Rajagopal, K.R., Antaki, J.F., 1998. The blood flow in tubes: theory and experiments. Mech. Res. Commun. 25, 257–262.